Supporting Information

Drescher et al. 10.1073/pnas.1019079108

SI Text

Hydrodynamics vs. Noise in Cell–Cell Scattering. Guided by our experimental results for *Escherichia coli*, we would like to estimate the relative importance of long-range hydrodynamics in cell–cell and cell–surface interactions. To this end, we compare the magnitude of hydrodynamic effects with orientational diffusion due to external noise and intrinsic variability in the bacterial swimming mechanism. To model the hydrodynamic interactions, we use a force dipole approximation to the experimentally determined flow field, as discussed in the main text. Rotational diffusion is quantified by the measured constant $D_r = 0.057$ rad^2/s.

We estimate the mean square change in swimming direction due to hydrodynamic interactions between two bacteria, assuming that the nearest encounter occurs at time $t = 0$ at a distance r. We further assume that a bacterium is approximately ellipsoidal (major axis length a, minor axis length b) and swims at constant speed V_0. If the unit vector $\boldsymbol{d}(t)$ denotes the swimming direction of a bacterium at time t, the mean square angular change of the swimming direction during the time interval $[-t/2,t/2]$ is given by

$$\langle \Delta\phi(t,r)^2\rangle_H := \langle \arccos[\boldsymbol{d}(-t/2)\cdot\boldsymbol{d}(t/2)]^2\rangle_H, \qquad [S1]$$

with $\langle\cdot\rangle_H$ indicating an average over all possible orientations and positions of binary encounters with minimal distance r.

To evaluate the importance of hydrodynamic interactions relative to random fluctuations, we compare $\langle \Delta\phi(t,r)^2\rangle_H$ with angular diffusion due to Brownian motion and intrinsic swimming variability in three dimensions (3D)

$$\langle \Delta\phi(t)^2\rangle_D = 4D_r t. \qquad [S2]$$

We can define an effective hydrodynamic radius r_H by means of the condition

$$\langle \Delta\phi(\tau,r_H)^2\rangle_H = \langle \Delta\phi(\tau)^2\rangle_D, \qquad [S3]$$

where τ is the characteristic interaction time scale. For scattering events with $r > r_H$ hydrodynamics becomes practically irrelevant. As we shall see below, the final result for r_H will be very robust against changes of the interaction time scale and other parameters.

To obtain an analytical estimate for $\langle \Delta\phi(\tau,r)^2\rangle_H$, we note that the hydrodynamic change of the unit orientation $\boldsymbol{d}(t)$ of an ellipsoidal bacterium is given by (1)

$$\dot{d}_i = \frac{1}{2}\epsilon_{ijk}\omega_j d_k + \Gamma d_k E_{kj}(\delta_{ji} - d_j d_i), \qquad [S4]$$

where the overdot indicates the time-derivative, ϵ_{ijk} is the Levi–Civita tensor, $\omega_i = \epsilon_{ijk}u_{k,j}$ is the vorticity of the fluid field $\boldsymbol{u}(\boldsymbol{r})$ at the position of the bacterium, $E_{ij} = (u_{i,j} + u_{j,i})/2$ is the rate-of-strain tensor, and $\Gamma = [(a/b)^2 - 1]/[(a/b)^2 + 1]$ is a geometry factor (we use a summation convention for equal vector and tensor indices, and abbreviate partial derivatives as $u_{i,j} := \partial u_i/\partial r_j$). Our experiments show that the flow field $\boldsymbol{u}(\boldsymbol{r})$ generated by a (second) bacterium with unit orientation vector $\boldsymbol{d}'$ is approximately dipolar,

$$u_i(\boldsymbol{r}) = \frac{A}{|\boldsymbol{r}|^2}[3(\hat{\boldsymbol{r}}\cdot\boldsymbol{d}')^2 - 1]\hat{r}_i, \qquad A = \frac{\ell F}{8\pi\eta}, \qquad \hat{\boldsymbol{r}} = \frac{\boldsymbol{r}}{|\boldsymbol{r}|}, \qquad [S5]$$

yielding

$$\omega_i = 6A\frac{(\hat{\boldsymbol{r}}\cdot\boldsymbol{d}')}{|\boldsymbol{r}|^3}\epsilon_{ijk}d'_j\hat{r}_k, \qquad [S6]$$

$$E_{ij} = \frac{A}{|\boldsymbol{r}|^3}\Big\{[3(\hat{\boldsymbol{r}}\cdot\boldsymbol{d}')^2 - 1]\delta_{ij} + 3(\hat{\boldsymbol{r}}\cdot\boldsymbol{d}')(d'_j\hat{r}_i + d'_i\hat{r}_j) - [15(\hat{\boldsymbol{r}}\cdot\boldsymbol{d}')^2 - 3]\hat{r}_i\hat{r}_j\Big\}. \qquad [S7]$$

Assuming the characteristic scattering time τ is sufficiently small, which is realistic for 3D scattering due to the relatively large swimming speeds of *E. coli*, we can approximate

$$\langle \Delta\phi(\tau,r)^2\rangle_H \simeq \tau^2\langle|\dot{\boldsymbol{d}}(0)|^2\rangle_H = 9(\Gamma+1)^2\frac{A^2\tau^2}{r^6}\langle(\hat{\boldsymbol{r}}\cdot\boldsymbol{d}')^2(\boldsymbol{d}\cdot\boldsymbol{d}')^2\rangle_H.$$

Assuming that $\hat{\boldsymbol{r}}$ is uniformly distributed on a sphere, and $\boldsymbol{d}$ uniformly distributed on a circle in the tangential plane at radius r, we obtain

$$\langle \Delta\phi(\tau,r)^2\rangle_H = \frac{3}{5}(\Gamma+1)^2\frac{A^2\tau^2}{r^6}. \qquad [S8]$$

Equating this expression with rotational diffusion (see Eq. **S3**) yields the effective hydrodynamic horizon

$$r_H \simeq \left[\frac{3}{20}(\Gamma+1)^2\frac{A^2\tau}{D_r}\right]^{1/6}. \qquad [S9]$$

Note that, due to the $\tau^{1/6}$ dependence, the result is rather insensitive to the particular value used for τ and, similarly, to changes in the other parameters. Adopting $\tau = a/V_0$ and inserting experimentally measured values (a,ℓ,F,V,D_r) as given in the main text, we obtain $r_H \simeq 3.3$ μm for *E. coli*. Eq. **S9** can be viewed as an upper bound, as the dipolar flow model overestimates $|\boldsymbol{u}|$ for $r < 6$ μm (see Fig. 1*D* in the main text).

We may thus conclude that (long-range) hydrodynamic interactions will only be of relevance if at least one of the following conditions is satisfied: (*i*) Bacterial suspensions are sufficiently dense; (*ii*) self-organization and/or external stimuli lead to orientational and positional correlations between nearby bacteria; (*iii*) rotational diffusion is strongly suppressed (e.g., through an increase of viscosity). However, our results imply that under natural conditions hydrodynamic long-range interactions are washed out by noise, suggesting that orientational order in dense bacterial suspensions is primarily caused by an interplay of swimming motility and short-range interactions (steric repulsion, lubrication effects, flagellar bundling, etc.) (2).

Hydrodynamic Interactions with a Wall. The previous section focused on the competition between noise and hydrodynamics in bacterial pairwise scattering. We now perform a similar analysis for the hydrodynamic interaction between a bacterium and a wall. Specifically, we are interested in the following two questions (3, 4):

- Is long-range hydrodynamics relevant for bacterial cell-surface scattering?
- Can hydrodynamics trap a bacterium near a wall—and, if so, for how long?

Long-Range Interaction with a Wall. We again approximate the flow field around *E. coli* by a force dipole flow. We denote the position of the dipole by $\boldsymbol{x}$, its normalized orientation vector (the bacterial swimming direction) by $\boldsymbol{d}$, and the unit normal vector of the solid boundary by $\boldsymbol{n}$ (pointing into the fluid). Using Blake's solution (5) for a Stokeslet near an infinite planar no-slip surface one can derive explicit expressions for the advective flow $u_i'(\boldsymbol{x})$, the vorticity $\omega_i'(\boldsymbol{x})$, and the symmetric rate-of-strain tensor $E_{ij}'(\boldsymbol{x})$, which act on a force dipole near a wall due to the interaction with its hydrodynamic image (5, 3):

$$u_j'(\boldsymbol{x}) = \frac{3A}{8h^2}\left\{2(\boldsymbol{n}\cdot\boldsymbol{d})d_j + [(\boldsymbol{n}\cdot\boldsymbol{d})^2 - 1]n_j\right\}, \qquad \textbf{[S10]}$$

$$\omega_k'(\boldsymbol{x}) = -\frac{3A}{4h^3}(\boldsymbol{n}\cdot\boldsymbol{d})\epsilon_{kni}n_i d_n, \qquad \textbf{[S11]}$$

$$E_{in}'(\boldsymbol{x}) = \frac{A}{16h^3}\Big\{[5(\boldsymbol{n}\cdot\boldsymbol{d})^2 - 1]\delta_{in} - 6d_i d_n - 12(\boldsymbol{n}\cdot\boldsymbol{d})(d_i n_n + n_i d_n) + 9[(\boldsymbol{n}\cdot\boldsymbol{d})^2 + 1]n_i n_n\Big\}, \qquad \textbf{[S12]}$$

where $h := |(\boldsymbol{x}.\boldsymbol{n})|$ denotes the orthogonal distance to the surface, assuming that the coordinate origin lies on the surface, and ϵ_{ijk} is the Levi–Civita tensor (primes are used to emphasize that the fields in Eqs. **S10**–**S12** contain only the image contribution; for clarity of notation, primes were omitted in the corresponding formulas in main text). Following Pedley and Kessler (1), the deterministic equations of motion for a dipole swimmer that moves at constant swimming speed V_0 in the presence of the wall are given by

$$\dot{x}_j = V_0 d_j + u_j'(\boldsymbol{x}), \qquad \textbf{[S13]}$$

$$\dot{d}_j = \frac{1}{2}\epsilon_{jkl}\omega_k' d_l + \Gamma d_i E_{in}'(\delta_{nj} - d_n d_j). \qquad \textbf{[S14]}$$

As before, $\Gamma = [(a/b)^2 - 1]/[(a/b)^2 + 1]$ is a geometric factor for ellipsoidal particles with major axis length a and minor axis length b. The equations **S14** for the orientation change can be explicitly written as

$$\dot{d}_j = \frac{3A}{8h^3}(\boldsymbol{n}\cdot\boldsymbol{d})\left\{1 - \frac{\Gamma}{2}[3(\boldsymbol{n}\cdot\boldsymbol{d})^2 - 1]\right\}[(\boldsymbol{n}\cdot\boldsymbol{d})d_j - n_j]. \qquad \textbf{[S15]}$$

To study whether or not long-range hydrodynamics affects the dynamics of a bacterium as it swims towards a wall, we numerically integrated Eqs. **S13** and **S14** using the experimentally determined parameters for the *E. coli* flow field. The results, which are summarized in Fig. 2 in the main text, show that due to the high swimming speeds of *E. coli*, hydrodynamic long-range interactions are not likely to play an important role in interactions with walls.

Escape from a Wall. An *E. coli*-like ("pusher") bacterium oriented parallel to a no-slip surface experiences a hydrodynamic attraction towards the surface (3). Orientational noise and swimming may counteract this attraction. We now estimate the typical time it takes for *E. coli* to escape from the wall, using the dipole model defined by Eqs. **S10**–**S15** to see whether such a model can explain the experimentally observed long residence times of bacteria swimming in close proximity to a solid boundary. This model overestimates the effects of hydrodynamics if bacteria come very close to the surface, so that the escape time estimates obtained below should be regarded as approximate upper bounds.

Let us assume that an inelastic collision has led to alignment of the bacterial swimmer parallel to the wall and that, subsequently, its orientation changes by means of rotational diffusion. We denote by θ the angle between the swimmer and the surface (i.e., $\theta = 0$ means parallel to the surface). The bacterium will be able to escape from the surface, if its swimming velocity component perpendicular to the surface, $V_0(\boldsymbol{d}\cdot\boldsymbol{n}) = V_0\sin\theta$, exceeds the hydrodynamic attraction from the image, $\boldsymbol{u}'\cdot\boldsymbol{n}$. Taking the scalar product of Eq. **S13** with the wall normal $\boldsymbol{n}$, and setting $\dot{\boldsymbol{x}}\cdot\boldsymbol{n}$ to zero, defines the escape angle θ_e by

$$\sin\theta_e = \Lambda[1\text{–}3(\sin\theta_e)^2], \qquad \Lambda = \frac{3A}{8h^2V_0}. \qquad \textbf{[S16]}$$

Solving for θ_e yields

$$\theta_e = \arcsin\left(\frac{-1 + \sqrt{1 + 12\Lambda^2}}{6\Lambda}\right). \qquad \textbf{[S17]}$$

Using the experimental values $A = 31.8\ \mu\text{m}^3/\text{s}$ and $V_0 = 22\ \mu\text{m/s}$ for *E. coli*, one finds that $\Lambda < 1$ for distances $h > 0.74\ \mu\text{m}$ from the wall; intuitively, the larger the distance from wall the smaller the required escape angle. This suggests that, typically, the escape angle will be small, $\theta_e \ll 1$. In this case, one can approximate

$$\theta_e \simeq \Lambda, \qquad \textbf{[S18]}$$

which becomes quite accurate for *E. coli* parameters when $h > 1.5\ \mu\text{m}$. As the dipole model considerably overestimates the actual flow field close to the surface, we can expect that generally $\theta_e \ll 1$.

To estimate the mean escape time, we next consider Eq. **S15** for the hydrodynamic torque. Due to the elongated shape of *E. coli*, we can approximate $\Gamma \simeq 1$, and thus find for the component perpendicular to the wall

$$\frac{d}{dt}\sin\theta = -\frac{9A}{16h^3}\sin\theta(\cos\theta)^4. \qquad \textbf{[S19]}$$

This can be rewritten as

$$\dot{\theta} = -\frac{d}{d\theta}U(\theta), \qquad \textbf{[S20]}$$

where the effective angular "potential" $U(\theta)$ is given by

$$U(\theta) = \frac{9A}{64h^3}[1 - (\cos\theta)^4] \qquad \textbf{[S21]}$$

and is normalized such that $U(0) = 0$. During an inelastic collision with the wall, the orientation of the bacterium aligns with the wall, implying that $\theta < \theta_e$. Because θ_e is typically small, as discussed above, one can use the harmonic approximation of the potential in Eq. **S21**,

$$U(\theta) \simeq \frac{\theta^2}{2\kappa}, \qquad \kappa = \frac{16h^3}{9A}, \qquad \textbf{[S22]}$$

where κ defines the characteristic time scale for hydrodynamic realignment in the dipole model.

Eqs. **S20** and **S21** capture the deterministic torque that acts on the bacterium due to its hydrodynamic image. To account for the stochastic effect of rotational diffusion, we may add a Langevin (6) term to Eq. **S20**, yielding

$$\dot{\theta} = -\frac{d}{d\theta}U(\theta) + (2D_r^*)^{1/2}\xi(t), \qquad \textbf{[S23]}$$

where D_r^* is the rotational diffusion constant close to the surface in the direction perpendicular to the surface, and $\xi(t)$ denotes

Gaussian white noise characterized by $\langle \xi(t) \rangle = 0$ and $\langle \xi(t)\xi(t') \rangle = \delta(t-t')$. In general, we expect D_r^* to be smaller than the "bare" diffusion constant D_r measured far from boundaries, due to geometric constraints on the bacterial orientation near a wall.

The Langevin Eq. **S23** describes overdamped (angular) Brownian motion in the effective potential $U(\theta)$. Therefore, the question how long a bacterium can be trapped close to a surface reduces to a Kramers problem (6, 7) for the escape over a potential barrier ΔU, which in our case is determined by the escape angle θ_e,

$$\Delta U = U(\theta_e). \qquad \textbf{[S24]}$$

If the hydrodynamic torque is small, corresponding to a low barrier $\Delta U \ll D_r^*$, the typical time of escape for a bacterium with initial condition $\theta(0) = 0$ is determined by the rotational diffusion time scale

$$t_r(h) \simeq \frac{\theta_e^2}{D_r^*}. \qquad \textbf{[S25]}$$

Using the harmonic approximation (Eq. **S22**) with $\theta_e \simeq \Lambda$, we may estimate from the condition $\Delta U = D_r^*$ the transition height

$$h_e = \frac{1}{2}\left(\frac{81}{16}\frac{A^3}{D_r^* V_0^2}\right)^{1/7}; \qquad \textbf{[S26]}$$

for $h > h_e$ hydrodynamic effects becomes practically irrelevant. Inserting our experimentally measured values for A, V_0 and the rotational diffusion constant far from surfaces D_r, we find

$$h_e = 1.7 \times \left(\frac{D_r}{D_r^*}\right)^{1/7} \ \mu\text{m}. \qquad \textbf{[S27]}$$

This means that even for a very small rotational diffusion constant $D_r* \ll D_r$, the torque exerted by the hydrodynamic image becomes practically negligible if the bacterium is more than a body length away from the surface.

For sufficiently high barriers $\Delta U \gg D_r^*$, standard arguments from transition state theory (6) imply that the mean escape time becomes modified from the rotational diffusion time t_r by an Arrhenius–Kramers factor, so that in this case approximately

$$t_e(h) \approx \left(\frac{\theta_e^2}{D_r^*}\right) \exp\left(\frac{\Delta U}{D_r^*}\right). \qquad \textbf{[S28]}$$

To gain some qualitative insight into the possibility of hydrodynamic trapping close to a surface, we rewrite Eq. **S28** in terms of h_e from Eq. **S26**, adopting as before the harmonic approximation of Eq. **S22** with $\theta_e \simeq \Lambda$. This leads to

$$t_e(h) \approx \left(\frac{32}{9}\right)\left(\frac{h_e^7}{Ah^4}\right) \exp\left[\left(\frac{h_e}{h}\right)^7\right], \qquad \textbf{[S29]}$$

which suggests the possibility of a very strong increase of the escape time due to hydrodynamic effects close to the surface.

In practice, Kramers formulas like Eq. **S28** often begin to work reasonably well if $\Delta U > 3D_r^*$. Again using the harmonic approximation of Eq. **S22** with $\theta_e \simeq \Lambda$, the condition $\Delta U = 3D_r^*$ yields

$$h_K = 1.5 \times \left(\frac{D_r}{D_r^*}\right)^{1/7} \ \mu\text{m}. \qquad \textbf{[S30]}$$

For *E. coli*, this is approximately the distance where the linear approximation $\theta_e \simeq \Lambda$ becomes valid, so that the right-hand side of Eq. **S29** can provide useful qualitative insight into the behavior of the escape time at distances $h \simeq h_K$, assuming that the dipole model still provides a reasonable approximation in this limit.

Using the quadratic expressions for ΔU with $\theta_e \simeq \Lambda$, and our experimentally measured values for *E. coli* to evaluate the escape time at a distance $h = 1.5$ μm from the wall, we find

$$t_e \approx 0.78 \times \left(\frac{D_r}{D_r^*}\right) \exp\left[1.99 \times \left(\frac{D_r}{D_r^*}\right)\right] \ \text{s}, \qquad \textbf{[S31]}$$

which suggests that bacteria can be temporarily trapped for several seconds, when they come sufficiently close to the surface. Note that, while the distance scales h_e and h_K are very robust to changes in D_r^*/D_r, the mean escape time t_e is very sensitive to variations of this ratio.

In summary, we may conclude that: (*i*) Hydrodynamics is practically irrelevant if the bacterium is more than a body length away from the surface; (*ii*) hydrodynamic effects could, at least partially, account for the experimentally observed long escape times of bacteria, when they swim very close (<2 μm) to a solid boundary. However, a more detailed understanding of the long residence times near walls is an important challenge that requires further studies of near-field interactions between bacteria and surfaces.

Spectral Decomposition of Bacterial Flow Fields. An expansion of the flow field $\boldsymbol{u}(\boldsymbol{r})$ in terms of vector spherical harmonics yields a systematic decomposition of the angular flow structure. We expect this approach, which is similar to the decomposition of quantum mechanical wave functions in terms of scalar spherical harmonics, to be useful in future studies that aim to classify the fluid flows of different microorganisms, and for comparing experimental data with theoretical models. After summarizing basic definitions, we will demonstrate the method first for dipolar test data and then also for the bacterial flow field measured in our experiments. The notation adopted in this part follows closely that of Hill (8).

Coordinates. It is convenient to consider a three-dimensional (3D) spherical coordinate system

$$r \in [0,\infty), \qquad \vartheta \in [0,\pi], \qquad \varphi \in [0,2\pi). \qquad \textbf{[S32]}$$

The radial coordinate r is defined relative to the center of the organism with the Cartesian $\hat{z}$-axis pointing along the swimming direction. The associated infinitesimal volume element takes the standard form

$$r^2 d\Omega := r^2 \sin\vartheta \, d\vartheta \, d\varphi, \qquad \textbf{[S33]}$$

and the locally orthonormal basis vectors of the spherical coordinate system $\{\hat{\boldsymbol{r}},\hat{\boldsymbol{\vartheta}},\hat{\boldsymbol{\varphi}}\}$ can be expressed in terms of the Cartesian unit vectors $\{\hat{\boldsymbol{x}},\hat{\boldsymbol{y}},\hat{\boldsymbol{z}}\}$ as

$$\hat{\boldsymbol{r}} = \sin\vartheta\cos\varphi\,\hat{\boldsymbol{x}} + \sin\vartheta\sin\varphi\,\hat{\boldsymbol{y}} + \cos\vartheta\,\hat{\boldsymbol{z}}, \qquad \textbf{[S34]}$$

$$\hat{\boldsymbol{\vartheta}} = \cos\vartheta\cos\varphi\,\hat{\boldsymbol{x}} + \cos\vartheta\sin\varphi\,\hat{\boldsymbol{y}} - \sin\vartheta\,\hat{\boldsymbol{z}}, \qquad \textbf{[S35]}$$

$$\hat{\boldsymbol{\varphi}} = -\sin\varphi\,\hat{\boldsymbol{x}} + \cos\varphi\,\hat{\boldsymbol{y}}. \qquad \textbf{[S36]}$$

Scalar Spherical Harmonics. The vector spherical harmonics discussed below can be most conveniently expressed in terms of the scalar spherical harmonics

$$Y_{lm}(\vartheta,\varphi) = \left[\frac{2l+1}{4\pi}\frac{(l-m)!}{(l+m)!}\right]^{1/2} P_{lm}(\mu) e^{im\varphi}, \qquad \textbf{[S37]}$$

where $\mu := \cos\vartheta$ and

$$P_{lm}(\mu) = (-1)^m \frac{(1-\mu^2)^{m/2}}{l!2^l} \frac{d^{l+m}}{d\mu^{l+m}} (\mu^2-1)^l \qquad \textbf{[S38]}$$

with $l = 0,1,2,\ldots$, and $m = -l, -l+1,\ldots,l$. The scalar spherical harmonics of Eq. **S37** satisfy the standard orthonormality relations

$$\int d\Omega\, Y_{lm} Y^*_{l'm'} = \delta_{ll'}\delta_{mm'}. \qquad \textbf{[S39]}$$

Vector spherical harmonics. Following Hill (8), we define vector spherical harmonics $\boldsymbol{V}_{lm}(\vartheta,\varphi)$, $\boldsymbol{W}_{lm}(\vartheta,\varphi)$, $\boldsymbol{X}_{lm}(\vartheta,\varphi)$ by

$$\boldsymbol{V}_{lm} := \left\{-\left(\frac{l+1}{2l+1}\right)^{1/2} Y_{lm}\right\}\hat{\boldsymbol{r}} + \left\{\frac{1}{[(l+1)(2l+1)]^{1/2}} \frac{\partial Y_{lm}}{\partial\vartheta}\right\}\hat{\boldsymbol{\vartheta}} + \left\{\frac{1}{[(l+1)(2l+1)]^{1/2}} \frac{1}{\sin\vartheta} \frac{\partial Y_{lm}}{\partial\varphi}\right\}\hat{\boldsymbol{\varphi}}, \qquad \textbf{[S40]}$$

$$\boldsymbol{W}_{lm} := \left\{\left(\frac{l}{2l+1}\right)^{1/2} Y_{lm}\right\}\hat{\boldsymbol{r}} + \left\{\frac{1}{[l(2l+1)]^{1/2}} \frac{\partial Y_{lm}}{\partial\vartheta}\right\}\hat{\boldsymbol{\vartheta}} + \left\{\frac{1}{[l(2l+1)]^{1/2}} \frac{1}{\sin\vartheta} \frac{\partial Y_{lm}}{\partial\varphi}\right\}\hat{\boldsymbol{\varphi}}, \qquad \textbf{[S41]}$$

$$\boldsymbol{X}_{lm} := \left\{\frac{i}{[l(l+1)]^{1/2}} \frac{1}{\sin\vartheta} \frac{\partial Y_{lm}}{\partial\varphi}\right\}\hat{\boldsymbol{\vartheta}} + \left\{-\frac{i}{[l(l+1)]^{1/2}} \frac{\partial Y_{lm}}{\partial\vartheta}\right\}\hat{\boldsymbol{\varphi}}, \qquad \textbf{[S42]}$$

with the additional convention $\boldsymbol{W}_{00} = \boldsymbol{X}_{00} \equiv \boldsymbol{0}$. For an arbitrary scalar function $f(r)$, we have (8)

$$\nabla\cdot(f\boldsymbol{V}_{lm}) = -\left(\frac{l+1}{2l+1}\right)^{1/2}\left(\frac{df}{dr} + \frac{l+2}{r}f\right)Y_{lm}, \qquad \textbf{[S43]}$$

$$\nabla\cdot(f\boldsymbol{W}_{lm}) = \left(\frac{l}{2l+1}\right)^{1/2}\left(\frac{df}{dr} - \frac{l-1}{r}f\right)Y_{lm}, \qquad \textbf{[S44]}$$

$$\nabla\cdot(f\boldsymbol{X}_{lm}) \equiv 0, \qquad \textbf{[S45]}$$

which implies that the functions $\boldsymbol{X}_{lm}$ are divergence-free

$$\nabla\cdot\boldsymbol{X}_{lm} \equiv 0. \qquad \textbf{[S46]}$$

The vector spherical harmonics from Eqs. **S40**–**S42** fulfill the following orthonormality relations

$$\int d\Omega\, \boldsymbol{V}_{lm}\cdot\boldsymbol{V}^*_{l'm'} = \delta_{ll'}\delta_{mm'}, \qquad \textbf{[S47]}$$

$$\int d\Omega\, \boldsymbol{W}_{lm}\cdot\boldsymbol{W}^*_{l'm'} = \delta_{ll'}\delta_{mm'}, \qquad \textbf{[S48]}$$

$$\int d\Omega\, \boldsymbol{X}_{lm}\cdot\boldsymbol{X}^*_{l'm'} = \delta_{ll'}\delta_{mm'}, \qquad \textbf{[S49]}$$

$$\int d\Omega\, \boldsymbol{V}_{lm}\cdot\boldsymbol{W}^*_{l'm'} = 0, \qquad \textbf{[S50]}$$

$$\int d\Omega\, \boldsymbol{V}_{lm}\cdot\boldsymbol{X}^*_{l'm'} = 0, \qquad \textbf{[S51]}$$

$$\int d\Omega\, \boldsymbol{W}_{lm}\cdot\boldsymbol{X}^*_{l'm'} = 0. \qquad \textbf{[S52]}$$

Hence, an arbitrary vector field $\boldsymbol{u}(r,\vartheta,\varphi)$ can be decomposed in the form

$$\boldsymbol{u}(r,\vartheta,\varphi) = \sum_{l=0}^{\infty}\sum_{m=-l}^{l} u^V_{lm}(r)\boldsymbol{V}_{lm} + \sum_{l=1}^{\infty}\sum_{m=-l}^{l} u^W_{lm}(r)\boldsymbol{W}_{lm} + \sum_{l=1}^{\infty}\sum_{m=-l}^{l} u^X_{lm}(r)\boldsymbol{X}_{lm}, \qquad \textbf{[S53]}$$

where the radial coefficient functions $u^\gamma_{lm}(r)$ with $\gamma = V, W, X$ are given by

$$u^V_{lm}(r) := \int d\Omega\, \boldsymbol{u}(r,\vartheta,\varphi)\cdot\boldsymbol{V}^*_{lm}(\vartheta,\varphi), \qquad \textbf{[S54]}$$

$$u^W_{lm}(r) := \int d\Omega\, \boldsymbol{u}(r,\vartheta,\varphi)\cdot\boldsymbol{W}^*_{lm}(\vartheta,\varphi), \qquad \textbf{[S55]}$$

$$u^X_{lm}(r) := \int d\Omega\, \boldsymbol{u}(r,\vartheta,\varphi)\cdot\boldsymbol{X}^*_{lm}(\vartheta,\varphi). \qquad \textbf{[S56]}$$

If the flow field $\boldsymbol{u}$ is a solution to the incompressible Stokes equations with pressure field p and viscosity η, which means that

$$\eta\nabla^2\boldsymbol{u} = \nabla p, \qquad \nabla\cdot\boldsymbol{u} \equiv 0, \qquad \textbf{[S57]}$$

then the coefficient functions $\{u^\gamma_{lm}(r)\}_{\gamma=V,W,X}$ are coupled through Eqs. **S57** and the specific boundary conditions that complement these equations.

Extracting Coefficient Functions from 2D Data. Eqs. **S53**–**S56** can be used to systematically decompose 3D flow field data into contributions from different harmonics. In practice, however, the presently available imaging data for bacteria and algae (9) is restricted to the 2D focal plane of the microscope, taken here to be the $(y=0)$-plane in which the organisms swims. To achieve systematic decomposition in terms of the vector spherical harmonics $\{\boldsymbol{V}_{lm}(\vartheta,\varphi), \boldsymbol{W}_{lm}(\vartheta,\varphi), \boldsymbol{X}_{lm}(\vartheta,\varphi)\}$ in this situation, it is necessary to make additional assumptions about the symmetry of the observed flow fields. For axially symmetric organisms far from boundaries the surrounding average fluid velocity field should be cylindrically symmetric with respect to their body axis $\hat{z}$, which means that

$$\boldsymbol{u}(r,\vartheta,\varphi) = R_z(\zeta)\boldsymbol{u}(r,\vartheta,\varphi+\zeta), \qquad \forall(r,\vartheta,\varphi,\zeta), \qquad \textbf{[S58]}$$

where the matrix

$$R_z(\zeta) = \begin{pmatrix} \cos\zeta & -\sin\zeta & 0 \\ \sin\zeta & \cos\zeta & 0 \\ 0 & 0 & 1 \end{pmatrix} \qquad \textbf{[S59]}$$

represents the rotation by an angle ζ about the $\hat{z}$-axis. In particular, we have in this case

$$\boldsymbol{u}(r,\vartheta,\varphi) = R_z(\varphi)\boldsymbol{u}(r,\vartheta,0), \qquad \textbf{[S60]}$$

where $\boldsymbol{u}(r,\vartheta,0)$ is the field measured in the focal $(y=0)$-plane. Defining

$$\bar{\boldsymbol{V}}_{lm}(\vartheta) := \int_0^{2\pi} d\varphi\, R_z(\varphi)\boldsymbol{V}_{lm}, \qquad \textbf{[S61]}$$

$$\bar{\boldsymbol{W}}_{lm}(\vartheta) := \int_0^{2\pi} d\varphi\, R_z(\varphi)\boldsymbol{W}_{lm}, \qquad \textbf{[S62]}$$

$$\bar{\boldsymbol{X}}_{lm}(\vartheta) := \int_0^{2\pi} d\varphi\, R_z(\varphi)\boldsymbol{X}_{lm}, \qquad \textbf{[S63]}$$

the expansion coefficients can be written as

$$u^V_{lm}(r) = \int_0^\pi d\vartheta \sin\vartheta\ \boldsymbol{u}(r,\vartheta,0)\cdot\bar{\boldsymbol{V}}^*_{lm}, \qquad \textbf{[S64]}$$

$$u^W_{lm}(r) = \int_0^\pi d\vartheta \sin\vartheta\ \boldsymbol{u}(r,\vartheta,0)\cdot\bar{\boldsymbol{W}}^*_{lm}, \qquad \textbf{[S65]}$$

$$u^X_{lm}(r) = \int_0^\pi d\vartheta \sin\vartheta\ \boldsymbol{u}(r,\vartheta,0)\cdot\bar{\boldsymbol{X}}^*_{lm}. \qquad \textbf{[S66]}$$

Eqs. **S64–S66** require knowledge of all three flow components u_x, u_y, u_z, in the $(y = 0)$-plane. In our experiments, we can only measure the flow components in the focal plane, and we therefore set $\boldsymbol{u}(r,\vartheta,0) = (u_x,0,u_z)$, cf. remarks below.

We next illustrate the spectral decomposition of the angular flow field structure for both numerically generated test data and real data from our experiments. To this end, we estimate the integrals in Eqs. **S64–S66** numerically using spatially discrete flow field data $\{\boldsymbol{u}(\boldsymbol{r}_i)\}$, specified on semicircles of constant radius $|\boldsymbol{r}_i| = r$, by replacing the integral over ϑ through trapezoidal Riemann sums with the discretization determined by the angular resolution of our data. Generally, the finer the angular resolution $\Delta\vartheta$, the more accurately one can estimate the radial coefficient functions $\{u^\gamma_{lm}(r)\}_{\gamma=V,W,X}$. More precisely, we need $N_\vartheta \gg l$, where $N_\vartheta(r)$ is the number of data grid points along the semicircle of radius r. The results presented below are based on a polar grid with angular resolution $\Delta\vartheta = 1°$, corresponding to $N_\vartheta(r) = 181$.

Test Case: Dipolar Flow Field. Our experiments show that the flow $\boldsymbol{u}(\boldsymbol{r})$ generated by an *E. coli* bacterium with unit orientation vector $\boldsymbol{d}$ is well-approximated by a force dipole flow, with components

$$u_i(\boldsymbol{r}) = \frac{A}{|\boldsymbol{r}|^2}[3(\hat{\boldsymbol{r}}\cdot\boldsymbol{d})^2 - 1]\hat{r}_i, \qquad \hat{\boldsymbol{r}} = \frac{\boldsymbol{r}}{|\boldsymbol{r}|}, \qquad \textbf{[S67]}$$

and dipole strength $A \simeq 31.8\ \mu m^3/s$. To illustrate the flow field decomposition by means of vector spherical harmonics, we first consider test data generated from the ideal force dipole field by computing the components $u_i(\boldsymbol{r})$ at different radii r on a polar grid with angular spacing $\Delta\vartheta = 1°$. The corresponding flow field for the swimmer orientation $\boldsymbol{d} = (0,0,1)$ is shown in Fig. S1*A*.

To verify our decomposition procedure, we can insert the coefficient functions $\{u^V_{lm}(r),u^W_{lm}(r),u^X_{lm}(r)\}$, as calculated from Eqs. **S64–S66**, into the expansion formula (Eq. **S53**) and compare the resulting flow field with the original velocity field $\boldsymbol{u}(\boldsymbol{r})$. The symbols in Fig. S1 *B* and *C* represent the components of the force dipole flow field at two different radii. The lines indicate the approximation by vector spherical harmonics, obtained with only a finite number of basis functions $\{\boldsymbol{V}_{l'm}(\vartheta,\varphi),\boldsymbol{W}_{l'm}(\vartheta,\varphi),\boldsymbol{X}_{l'm}(\vartheta,\varphi)\}$ with $0 \le l' \le l$. As evident from Fig. S1 *B* and *C*, the quality of the fit to the exact flow data gradually improves the more harmonics one includes. Generally, we find that for $N_\vartheta(r) = 181$ the exact flow field (Eq. **S53**) is well-approximated when including spherical harmonics with $l' \le 5$, see Fig. S1 *B* and *C*.

Experimental Case: Bacterial Flow Field. We now apply an analogous analysis to the experimentally measured flow field, which is shown in Fig. S1*D*. The corresponding results are summarized in Fig. S1 *E* and *F*. By comparing the diagrams in Fig. S1 *E* and *F* with their dipolar counterparts in Fig. S1 *B* and *C*, one readily observes considerable deviations from the dipolar structure for small distances $r \lesssim 6\ \mu m$, because the anterior-posterior symmetry is broken by the presence of the flagellar bundle. Generally, the decomposition in terms of vector spherical harmonics yields a systematic fitting procedure even at larger distances from the bacterium, when the experimental data becomes noisier, as evident from Fig. S1*F*.

Angular Kinetic Energy Spectra. The coefficient functions $\{u^V_{lm}(r), u^W_{lm}(r),u^X_{lm}(r)\}$ encode the full radial and angular structure of the bacterial flow field. To obtain a condensed, spectral representation of the flow field structure, we can integrate the local kinetic energy $|\boldsymbol{u}(\boldsymbol{r})|^2$ of the flow field over a surface of constant radius r. Using the orthonormality of the vector spherical harmonics, one then finds that the spectral functions

$$p_l(r) := \sum_{m=-l}^{l}[|u^V_{lm}(r)|^2 + |u^W_{lm}(r)|^2 + |u^X_{lm}(r)|^2] \qquad \textbf{[S68]}$$

measure the average kinetic energy generated by the microorganism at distance r in the angular mode l. The p_l-representation is conceptually similar to the angular power spectrum representation of the cosmic microwave background radiation (10). Fig. 2 shows the p_l-spectra for the dipolar test case and the bacterial flow field at different radii. One readily observes that the front-back asymmetry of the *E. coli* flow field results in an excitation of higher l-modes that are absent for a pure force dipole field. Generally, p_l-spectra can be useful for identifying and quantifying similarities and differences in the flow fields of different types of microorganisms, and for comparing them with theoretical models.

Remarks. The expansion in Eq. **S53** provides a useful tool for analyzing the angular structure of flow fields around microorganisms far from boundaries. This opens up the possibility to systematically categorize and compare the flow fields of different bacterial and algal species in terms of their angular vector spectra. While our experimental setup allows us to determine the velocity field only in the 2D focal plane, advanced future experiments might eventually be able to resolve the full 3D flow structure. If this can be achieved, then the additional symmetry assumptions underlying Eqs. **S64–S66** can be dropped, and the radial coefficient functions $\{u^V_{lm}(r),u^W_{lm}(r),u^X_{lm}(r)\}$ can be computed directly from Eqs. **S54–S56**. In principle, one could further decompose the radial coefficient functions in terms of a suitably chosen orthonormal basis system on $[0,\infty)$. The choice of the radial basis functions should be guided by the radial structure of known solutions to the Stokes equations (11).

1. Pedley TJ, Kessler JO (1992) Hydrodynamic phenomena in suspensions of swimming microorganisms. *Annu Rev Fluid Mech* 24:313–358.
2. Aranson IS, Sokolov A, Kessler JO, Goldstein RE (2007) Model for dynamical coherence in thin films of self-propelled microorganisms. *Phys Rev E Stat Nonlin Soft Matter Phys* 75:040901.
3. Berke AP, Turner L, Berg HC, Lauga E (2008) Hydrodynamic attraction of swimming microorganisms by surfaces. *Phys Rev Lett* 101:038102.
4. Li G, Tang JX (2009) Accumulation of microswimmers near a surface mediated by collision and rotational brownian motion. *Phys Rev Lett* 103:078101.
5. Blake JR, Chwang AT (1974) Fundamental singularities in viscous flow. *J Eng Math* 8:23–29.
6. Hänggi P, Talkner P, Borkovec M (1990) Reaction-rate theory: Fifty years after Kramers. *Rev Mod Phys* 62:251–341.
7. Dunkel J, Ebeling W, Schimansky-Geier L, Hänggi P (2003) Kramers problem in evolutionary strategies. *Phys Rev.* E67:061118
8. Hill EL (1954) The theory of vector spherical harmonics. *Amer J Phys* 22:211–214.
9. Drescher K, et al. (2010) Direct measurement of the flow field around swimming microorganisms. *Phys Rev Lett* 105:168101.
10. Spergel DN, et al. (2007) Three-year Wilkinson microwave anisotropy probe (WMAP) observations: Implications for cosmology. *Astrophys J* 170:377–408.
11. Happel J, Brenner H (1983) *Low Reynolds Number Hydrodynamics* (Martinus Nijhoff, The Hague).

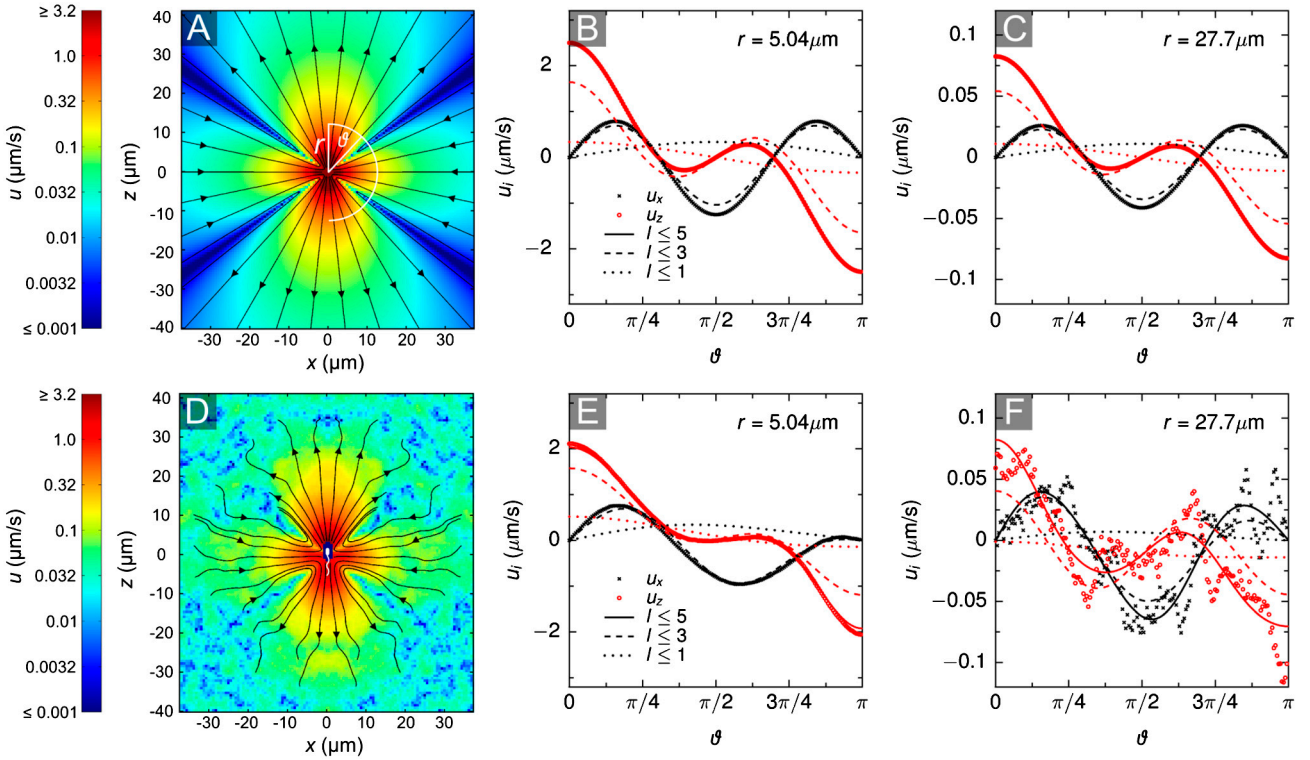

Fig. S1. Decomposition of the angular flow field structure in terms vector spherical harmonics for dipolar test data (*A*–*C*) and experimentally measured flow field of *E. coli* (*D*–*F*) at different radii *r*. (*A*) Test data sampled from the force dipole flow field of Eq. **S67** with amplitude $A = 31.8\ \mu m^3/s$ in the $(y = 0)$-plane. The swimmer is located at the origin and swims in the positive *z*-direction $\boldsymbol{d} = (0,0,1)$. Colors encode the flow field magnitude; arrows indicate local flow directions. (*B* and *C*) Angular flow profile at constant distance *r* from the swimmer, where the angle ϑ is measured clockwise with respect to the positive *z*-axis (see *A*), including basis functions with $0 \le l \le 5$. The fit (lines) to the sampled test data (symbols) improves when higher harmonics (i.e., higher values of *l*) are included. (*D*) Experimentally measured flow field in the $(y = 0)$-plane far from surfaces. The bacterium is located at the origin and swims in the positive *z*-direction. Colors encode flow field magnitude; arrows indicate local flow directions. (*E*) Angular flow profile at constant distance *r* from the bacterium. The fit to the experimental data (symbols) improves again when higher harmonics are included. By comparing with *B*, we observe a broken anterior-posterior symmetry at short-to-intermediate distances due the presence of the flagellar bundle. (*F*) At larger distances the experimental data becomes noisier; nevertheless the decomposition in terms of vector spherical harmonics yields a systematic fitting procedure.

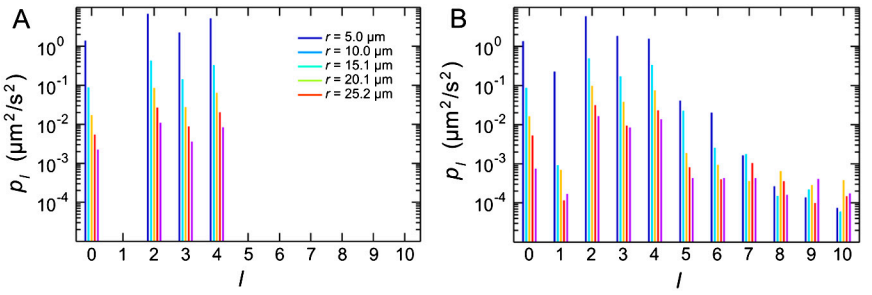

Fig. S2. Angular kinetic energy spectra for (*A*) the dipolar test model with amplitude $A = 31.8\ \mu m^3/s$, and (*B*) the experimentally determined flow field data for *E. coli*. The front-back asymmetry of the *E. coli* flow field results in an excitation of higher *l*-modes.